SAND2020-2426C

Evolution of Microstructural Descriptors in Elastomeric Foam During Uniaxial Compression

Sharlotte L.B. Kramer[1], Dan S. Bolintineanu[2], Enrico C. Quintana[3], Robert F. Waymel[1], and Kevin N. Long[4]

[1] Experimental Environment Simulation Department

[2] Fluid and Reactive Processes Department

[3] Nondestructive Environments and Diagnostics Department

[4] Computational Material Mechanics Department

Sandia National Laboratories, Albuquerque, NM 87185

ABSTRACT

In this work, we studied microstructural features of several densities of elastomeric polyurethane foams as they underwent uniaxial compression. High-resolution (1.725 micron/voxel) volumetric images of the foam samples were acquired using x-ray computed tomography at the Advanced Photon Source at Argonne National Laboratory. A custom-built quasi-static load frame that was transmissive to x-rays allowed in-situ volume acquisition at several levels of deformation ranging from 0-75% engineering strain. A wide range of statistical descriptors (e.g. pore size and shape distribution, spatial correlations, ligament thickness and curvature) were calculated at each deformation step. By performing a spatially averaged calculation using the pore size and shape, the change in pore anisotropy (i.e., the amount of deviation from a spherical pore) was calculated between deformation steps. In addition, relationships between globally averaged statistical descriptors and macroscale measurements were investigated. Digital volume correlation was used to calculate the volumetric strain field in each sample and enabled correlations between the locally measured statistical descriptors and local strain fluctuations to be explored. These data have inspired development of a new constitutive model that takes into account the effect of the local microstructure on the homogenized response.

Keywords: Foam, computed tomography, statistical descriptors, digital volume correlation, anisotropy

INTRODUCTION

Elastomeric foams are lightweight, inexpensive materials with a wide variety of uses from structural components to soft pad materials. Variations in foam density and polymer cross-linking can produce a broad range of material properties, ranging from highly flexible elastomers to rigid foams. In most manufacturing processes, cells are elongated along the direction of foam rise, resulting in anisotropic material properties. Another perspective is that a foam is merely a polymer with a particular microstructure of holes, and the interplay between solid polymer properties and microstructure govern the behavior of the foam. For low density foams (~50 kg/m^3), Gibson and Ashby [1] have advanced a successful theoretical framework relating bulk mechanical response to microstructural characteristics using beam analysis of idealized cell geometries. Theoretical, computational and experimental investigations of microstructure have been reported for low-density foams [2-10]; however, relatively few studies [11, 12, 13] have focused on moderate-density foams, where the microstructure is not well described by thin struts that form the edges of polyhedral cells. The relatively widespread availability of X-ray computed tomography (XCT) systems has spurred studies of microstructure in both metal [14, 15, 16] and polymer [11-13, 17] foams, as reviewed by Petit et al [18]. Anisotropy has been quantified in undeformed foam samples [19, 20] and compared between undeformed samples and samples deformed up to 7.5% axial strain [21]. However, to our knowledge, three-dimensional anisotropy evolution during deformation has not been previously characterized, particularly for the moderate-density foams and large deformations investigated here.

We studied the evolution of microstructure under large compressive deformation for different densities (hence different microstructures) of the same polymer matrix material, thus holding the solid material variable constant to isolate the microstructural effects. In this paper, we will present the in-situ x-ray computed tomography (XCT) at the Advance Photon Source (APS) at Argonne National Laboratory during compressive loading of different densities of General Plastics LAST-A-FOAM®, a flexible polyurethane foam. We will discuss statistical descriptors that quantify the microstructure, specifically the anisotropy, and the evolution of the descriptors with large deformation (0 to 75% engineering strain). We also performed digital volume correlation (DVC) on the XCT scans to quantify local strains through the volume and compare those to the statistical descriptors.

EXPERIMENTAL APPROACH

We performed uniaxial compression on 6.25-mm diameter, 6.25-mm tall cylinders of four densities of LAST-A-FOAM®, ranging from 80 to 240 kg/m^3. High-resolution (1.725 micron/voxel) radiographic images of the foam samples were acquired for tomographic reconstruction at varying steps of compression loading process. A custom-built quasi-static load frame that was transmissive to x-rays allowed in-situ volume acquisition at several levels of deformation ranging from 0-75% engineering strain; the frame was held in displacement control at specific displacement levels during approximately 12-minute x-ray scan times. Figure 1 shows a representative compressive engineering stress vs. compressive engineering strain for the 240 kg/m^3 foam for compression along the rise direction of the foam, comparing the APS discrete data to conventional servo-hydraulic load frame data for the loading-unloading behavior, and a central vertical slice of the foam in its undeformed state and two deformed states. The APS stress-strain behavior of the foam was similar to that of the conventional constant loading rate (0.001/s) data, with and initial elastic response, a post-yield/buckling plateau region, and a densification/lock-up regime. The central vertical slices show the considerable deformation and local evolution of the microstructure, with the 63% engineering strain in the densification region exhibiting the packing out of the porosity.

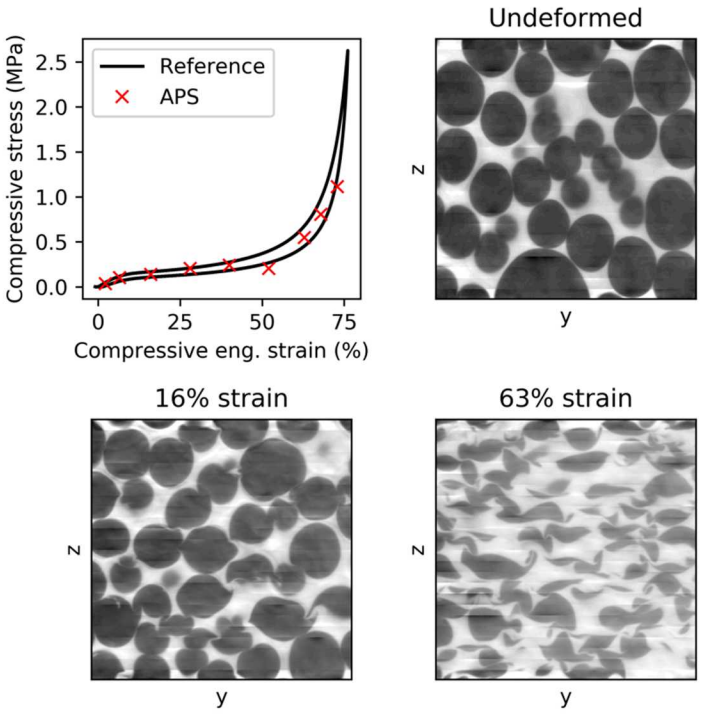

Figure 1: APS stress-strain and in-situ XCT data at various load levels for the 240-kg/m^3 foam aligning the rise direction with compressive load: (upper left) compressive engineering stress vs. compressive engineering strain, comparing the APS discrete data to conventional servo-hydraulic load frame data for the loading-unloading behavior; (upper right) central vertical slice of the XCT reconstruction at the

undeformed state; (lower left) central vertical slice of the XCT reconstruction at 16% strain in the plateau regime; and (lower right) central vertical slice of the XCT reconstruction at 63% strain in the early densification regime.

ANALYSIS

We measure anisotropy using a method for quantifying the shape of the autocorrelation function (ACF) of the grayscale three-dimensional image; this has the advantage of working directly with the grayscale image stack resulting from reconstruction of the X-ray projections as opposed of pore/matrix-identified, thresholded images. The spatial autocorrelation of the image intensity is defined as follows:

$$A(r) = \frac{\langle I(x+r)\, I(x)\rangle - \langle I(x)\rangle^2}{\langle I(x) - \langle I(x)\rangle\rangle^2}$$

Here, I(x) is the spatially varying grayscale intensity, and angular brackets ⟨⟩ denote a spatial average over all coordinate points x. The second term in the numerator is the mean intensity squared, and the denominator is equivalent to the variance of intensity. This shift and normalization are needed to adjust for changes in the dynamic range or shifts in detector sensitivity, allowing for a more meaningful comparison across different scans. To provide some physical intuition, the autocorrelation A(r) can be interpreted as the strength of correlation between intensities of any two points separated by vector r, averaged over all such pairs of points. Its limits are instructive: when $r = \|r\| \to 0$, $A(r) \to 1$, since every point is perfectly correlated with itself. Conversely, $r \to \infty$ implies $A(r) \to 0$, since the intensities of points separated by a sufficiently large distance are not expected to be correlated in a random medium. We measure overall anisotropy by quantifying the deviation of the shape of the ACF from a sphere, and its associated direction. This resembles the method proposed by Wald et al [22] in quantifying anisotropy of trabecular bone structure. The degree of anisotropy is defined based on the ratio of the smallest and largest eigenvalues of moment of inertia tensor of the ACF: $a_o = 1-\lambda_{min}/\lambda_{max}$. For cases where material structure does not possess an axis of symmetry (e.g. a sample compressed in the transverse direction), the shape of the ACF is orthotropic, with different dimensions in all three principal directions. In this case, a secondary direction of anisotropy exists, and its associated degree of anisotropy is defined as: $a_1 = 1-\max(\lambda_{min}/\lambda_{mid}, \lambda_{mid}/\lambda_{max})$, where λ_{mid} is the intermediate eigenvalue of the moment of inertia tensor of the ACF.

Figure 2 shows the anisotropy evolution with deformation for the 136 kg/m^3 and 240 kg/m^3 foams compressed along both the rise and transverse directions of the foams [Note: this data comes from in-situ XCT experiments taken on a benchtop system at Sandia National Laboratories, but for the same source foams as those tested at APS]. As expected for compression along the rise direction for both densities, the degree of anisotropy is moderately high, then reduces to nearly one as the pore shapes become nearly spherical, and then increases again with further deformation. For compression along the transverse direction, the level of anisotropy increases with deformation, given that the ellipsoidal pores are only becoming more eccentric with deformation. When comparing the anisotropy evolution of the two densities, we see that the anisotropy of the lower density begins at a higher anisotropy and ends at a lower anisotropy than that of the higher density foams. Also, the character of the anisotropy evolution is considerably different for the two densities for both foam orientations.

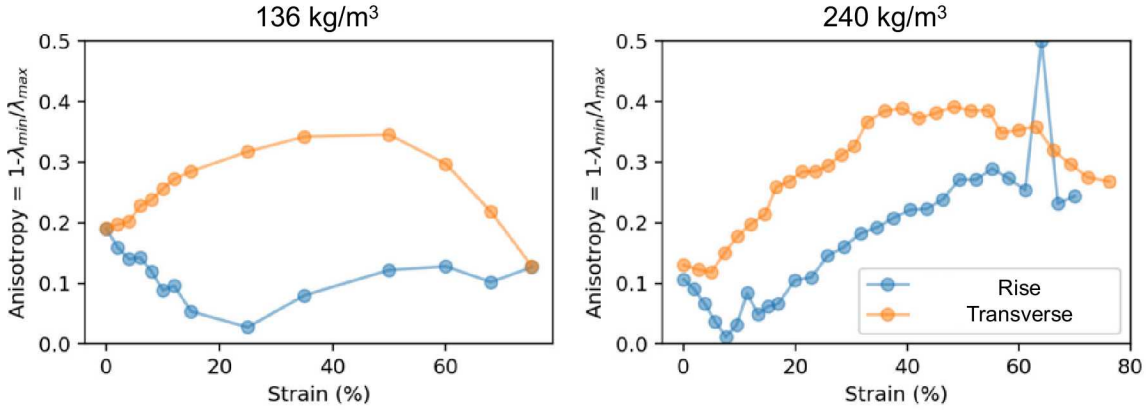

Figure 2: Anisotropy evolution of foams compressed along the rise and transverse orientations of two different foam densities, 136 and 240 kg/m^3, as a function of compressive engineering strain.

Along with this evolution of the anisotropy statistical descriptor that provides a homogenized measure of the local microstructural evolution with deformation, we performed DVC on the XCT scans of these foams under compression, using the foam pores as the volumetric features for the DVC algorithm. We utilized Correlated Solutions Vic-Volume to measure the local strain information on the internal response of the foam to the compressive load. A subset size of 151 and a step size of 30 were selected based on the average feature size within the volume. For the strain analysis, the smallest filter size, 5, was utilized. Figure 3 shows the engineering strain map for a central section of the foam at a nominal strain level of approximately 16%. The average engineering strain calculated for the volume form the DVC was 19%. There are areas within the volume that do see higher strain values than the average. Further analysis should indicate if these higher strain values correspond to any microstructural features that will allow for more accurate prediction of polymer foam behavior.

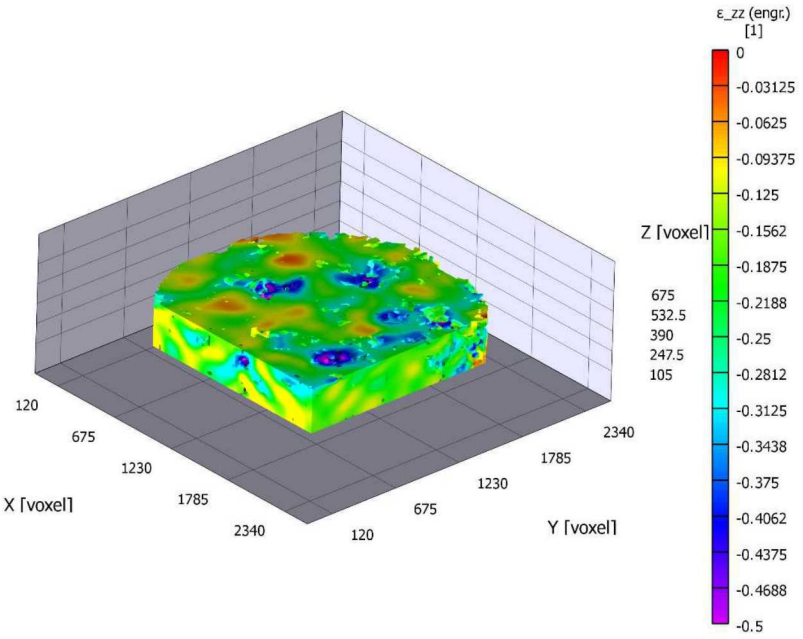

Figure 3: DVC result showing engineering strain distribution through the volume. The average engineering strain measured for the entire volume was 19% (Correlation uncertainty = 7%)

CONCLUSION

We presented quantified measures of microstructural evolution in moderate-density polymeric foams under uniaxial deformation with in-situ XCT from APS. We showed that anisotropy evolution differed between compression in the rise and transverse foam directions and between relative foam densities. DVC measurements of the volumetric stain corroborated the global average strain measured and showed regions of strain localization within the volume that can be correlated with microstructural features. Overall, this research has quanitified how microstructure influences the global and local behavior of polymeric foams under compression.

ACKNOWLEDGEMENTS

Supported by the Laboratory Directed Research and Development program at Sandia National Laboratories, a multi-mission laboratory managed and operated by National Technology & Engineering Solutions of Sandia, LLC, a wholly owned subsidiary of Honeywell International, Inc., for the U.S. Department of Energy's National Nuclear Security Administration under contract DE-NA0003525.

This research used resources of the Advanced Photon Source, a U.S. Department of Energy (DOE) Office of Science User Facility operated for the DOE Office of Science by Argonne National Laboratory under Contract No. DE-AC02-06CH11357.

REFERENCES

[1] L. J. Gibson, M. F. Ashby, Cellular solids: structure and properties, Cambridge university press, 1999.
[2] A. Huber, L. Gibson, Anisotropy of foams, Journal of Materials Science 23 (8) (1988) 3031–3040.
[3] M. D. Montminy, A. R. Tannenbaum, C. W. Macosko, The 3d structure of real polymer foams, Journal of colloid and interface science 280 (1) (2004) 202–211.
[4] L. Gong, S. Kyriakides, W.-Y. Jang, Compressive response of open-cell foams. part i: Morphology and elastic properties, In- ternational Journal of Solids and Structures 42 (5-6) (2005) 1355–1379.
[5] A. Brydon, S. Bardenhagen, E. Miller, G. Seidler, Simulation of the densification of real open-celled foam microstructures, Journal of the Mechanics and Physics of Solids 53 (12) (2005) 2638–2660.
[6] Y. Gan, C. Chen, Y. Shen, Three-dimensional modeling of the mechanical property of linearly elastic open cell foams, Inter- national Journal of Solids and Structures 42 (26) (2005) 6628– 6642.
[7] K. Li, X.-L. Gao, G. Subhash, Effects of cell shape and strut cross-sectional area variations on the elastic properties of three- dimensional open-cell foams, Journal of the Mechanics and Physics of Solids 54 (4) (2006) 783–806.
[8] W.-Y. Jang, A. M. Kraynik, S. Kyriakides, On the microstructure of open-cell foams and its effect on elastic properties, Inter- national Journal of Solids and Structures 45 (7-8) (2008) 1845–1875.
[9] A. Burteau, F. NGuyen, J.-D. Bartout, S. Forest, Y. Bienvenu, S. Saberi, D. Naumann, Impact of material processing and deformation on cell morphology and mechanical behavior of polyurethane and nickel foams, International Journal of Solids and Structures 49 (19-20) (2012) 2714–2732.
[10] S. Gaitanaros, S. Kyriakides, A. M. Kraynik, On the crushing of polydisperse foams, European Journal of Mechanics-A/Solids 67 (2018) 243–253.
[11] B. M. Patterson, K. Henderson, Z. Smith, Measure of morpho- logical and performance properties in polymeric silicone foams by x-ray tomography, Journal of Materials Science 48 (5) (2013) 1986–1996.
[12] B. M. Patterson, K. Henderson, R. D. Gilbertson, S. Tornga, N. L. Cordes, M. E. Chavez, Z. Smith, Morphological and performance measures of polyurethane foams using x-ray CT and mechanical testing, Microscopy and Microanalysis 20 (4) (2014) 1284–1293.
[13] B. M. Patterson, N. L. Cordes, K. Henderson, J. J. Williams, T. Stannard, S. S. Singh, A. R. Ovejero, X. Xiao, M. Robin- son, N. Chawla, In situ x-ray synchrotron tomographic imaging during the compression of hyper-elastic polymeric materials, Journal of materials science 51 (1) (2016) 171–187.
[14] Y. Hangai, K. Takahashi, R. Yamaguchi, T. Utsunomiya, S. Kitahara, O. Kuwazuru, N. Yoshikawa, Nondestructive observation of pore structure deformation behavior of functionally graded aluminum foam by x-ray computed tomography, Materials Science and Engineering: A 556 (2012) 678–684.
[15] M. Kader, M. Islam, M. Saadatfar, P. Hazell, A. Brown, S. Ahmed, J. Escobedo, Macro and micro collapse mechanisms of closed-cell aluminium foams during quasi-static compression, Materials & Design 118 (2017) 11–21.
[16] M.Saadatfar, M.Mukherjee, M.Madadi, G.Schro¨der-Turk, F. Garcia-Moreno, F. Schaller, S. Hutzler, A. Sheppard, J. Ban- hart, U. Ramamurty, Structure and deformation correlation of closed-cell aluminium foam subject to uniaxial compression, Acta materialia 60 (8) (2012) 3604–3615.
[17] N. Daphalapurkar, J. Hanan, N. Phelps, H. Bale, H. Lu, Tomography and simulation of microstructure evolution of a closed-cell polymer foam in compression, Mechanics of advanced materials and structures 15 (8) (2008) 594–611.
[18] C. Petit, S. Meille, E. Maire, Cellular solids studied by x-ray tomography and finite element modeling–a review, Journal of Materials Research 28 (17) (2013) 2191–2201.
[19] F. De Pascalis, M. Nacucchi, M. Scatto, R. Albertoni, Quantitative characterisation of low-density, high performance poly- meric foams using high resolution x-ray computed tomography and laser confocal microscopy, NDT & E International 83 (2016) 123–133.
[20] A.-H. Benouali, L. Froyen, T. Dillard, S. Forest, F. Nguyen, Investigation on the influence of cell shape anisotropy on the mechanical performance of closed cell aluminium foams using micro-computed tomography, Journal of materials science 40 (22) (2005) 5801–5811.
[21] F. De Pascalis, M. Nacucchi, Relationship between the anisotropy tensor calculated through global and object measurements in high-resolution x-ray tomography on cellular and composite materials, Journal of Microscopy 273 (1) (2019) 65– 80.
[22] M. J. Wald, B. Vasilic, P. K. Saha, F. W. Wehrli, Spatial autocorrelation and mean intercept length analysis of trabecular bone anisotropy applied to in vivo magnetic resonance imaging, Medical physics 34 (3) (2007) 1110–1120.